

# An Orthonormal Basis of Directional Haar Wavelets on Triangles

Jens Krommweh

**Abstract.** In order to get an efficient representation of images which contain orientated edges we construct a directional wavelet basis for  $L^2(\mathbb{R}^2)$ . The wavelets basis consists of Haar wavelets with compact support on triangles. In comparison with the classical wavelet transform our functions offer two more directions (diagonal directions). Applying our simple wavelet system to image denoising and approximation we observe suprisingly good results.

**Mathematics Subject Classification (2000).** Primary 42C40; Secondary 41A30, 65T60, 68U10, 94A08.

**Keywords.** directional Haar wavelet, multiwavelets, composite dilation wavelets, triangulations, image processing, approximation, denoising.

## 1. Introduction

Traditional wavelets are not very effective in dealing with images that contain orientated discontinuities (edges). To achieve a more efficient representation one has to use basis elements with much higher directional sensitivity. In recent years several approaches like curvelets [2], contourlets [3], and shearlets [5] have been studied providing essentially optimal approximation properties for images that are piecewise smooth and have discontinuities along  $C^2$ -curves. While curvelets and shearlets have compact support in frequency domain, in [8] we have constructed directional wavelet frames generated by functions with compact support in time domain. As in [7], our Haar wavelet constructions can be seen as special composite dilation wavelets [6], being based on a generalized multiresolution analysis (MRA) associated with a dilation matrix and a finite collection of 'shear' matrices. More precisely, the wavelet system in [8] is based on 16 mother scaling functions that are characteristic functions on triangles in the square  $[-1, 1]^2$ . Therefore the non-separable wavelets are able to detect eight different directions. In this paper

we consider a very similar multiwavelet construction, but based on 8 mother scaling functions only. Thus, we get not only a wavelet frame but even an orthonormal basis (ONB), which leads to fast and easy implementations. The price we have to pay is the loss of 4 directions. But we will see that the wavelet basis with four orientations gives good results in application. Our construction corresponds with that in [7] but it has been developed independently. While the main construction is similar an essential difference is the usage of another dilation matrix. Instead of the Quincunx matrix we use the isotropic dilation matrix  $A = 2I$ .

The paper is organized as follows. Firstly, we construct with a geometrical approach the scaling functions and directional ONB wavelets with compact support on triangles. In the second part of this paper we apply our basis functions to image processing. We will see that the simple and fast implementation leads to quite good results in denoising and approximation of images.

## 2. Construction of Haar-like scaling functions and corresponding wavelets

We consider the domain  $\Omega := [-\frac{1}{2}, \frac{1}{2}]^2$  and divide it into 8 triangles with the same area, see Figure 1(a). We want to introduce a vector of characteristic functions on these 8 triangles. Let the first non-separable scaling function  $\phi_0$  be a characteristic function on the triangle

$$U_0 = \text{conv}\left\{\begin{pmatrix} 0 \\ 0 \end{pmatrix}, \begin{pmatrix} 1/2 \\ 1/2 \end{pmatrix}, \begin{pmatrix} 0 \\ 1/2 \end{pmatrix}\right\} := \{x \in \mathbb{R}^2 : 0 \leq x_2 \leq \frac{1}{2}, 0 \leq x_1 \leq x_2\},$$

i.e.,

$$\phi_0(x) = \phi_0(x_1, x_2) := \chi_{U_0}(x_1, x_2) = \chi_{[0,1]}(\frac{x_1}{x_2}) \cdot \chi_{[0, \frac{1}{2}]}(x_2).$$

Let us apply the group of isometries of the square,

$$\mathcal{B} := \{B_i : i = 0, \dots, 7\} = \left\{ \pm \begin{pmatrix} 1 & 0 \\ 0 & 1 \end{pmatrix}, \pm \begin{pmatrix} 0 & 1 \\ 1 & 0 \end{pmatrix}, \pm \begin{pmatrix} 0 & -1 \\ 1 & 0 \end{pmatrix}, \pm \begin{pmatrix} 1 & 0 \\ 0 & -1 \end{pmatrix} \right\}.$$

Then, for  $i = 0, \dots, 7$  we have  $U_i := \{B_i^{-1}x : x \in U_0\} = B_i^{-1}U_0$ , and we define the further scaling functions  $\phi_i$  by

$$\phi_i(x) := \phi_0(B_i x) = \chi_{U_0}(B_i x) = \chi_{B_i^{-1}U_0}(x) = \chi_{U_i}(x),$$

$i = 0, \dots, 7$ . We consider now the sequence of spaces  $\{V_j\}_{j \in \mathbb{Z}}$  given by

$$V_j := \text{clos}_{L^2(\mathbb{R}^2)} \text{span}\{\phi_{i,j,k} : i = 0, \dots, 7; k \in \mathbb{Z}^2\}$$

with

$$\phi_{i,j,k}(x) := 2^{j+1} \sqrt{2} \phi_0(B_i(2^j x - k)), \quad i = 0, \dots, 7, k \in \mathbb{Z}^2,$$

where the factor  $2^{j+1} \sqrt{2}$  normalizes the scaling functions such that  $\langle \phi_{i,j,k}, \phi_{i',j',k'} \rangle = \delta_{i,i'} \delta_{j,j'} \delta_{k,k'}$ . Note that these functions can be understood as scaling functions with composite dilations (see [6, 10]). It is obvious that by construction  $\{V_j\}_{j \in \mathbb{Z}}$  forms a stationary MRA of  $L^2(\mathbb{R}^2)$ , that can also be interpreted as a so-called ONB  $AB$ -MRA with  $A = 2I$  and  $B \in \mathcal{B}$  as introduced in [6, 10].

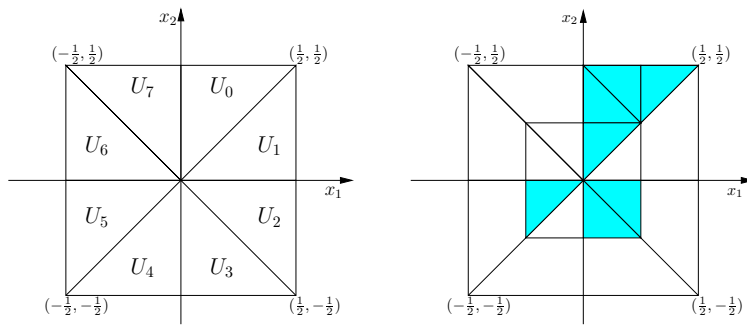


FIGURE 1. Scaling functions. (a) level  $V_0$ , (b) refinements of  $U_0$ .

Particularly, the scaling functions satisfy refinement equations. Using a vector notation  $\Phi := (\phi_0, \dots, \phi_7)^T$  the two-scale equation is given for every  $i = 0, \dots, 7$ ,  $j \in \mathbb{Z}$ , and  $k \in \mathbb{Z}^2$  by

$$\Phi(x) = 2 \sum_{k \in \mathbb{Z}^2} M_k^0 \Phi(2x - k), \quad x \in \mathbb{R}^2,$$

where  $M_k^0$  are  $8 \times 8$ -matrices containing only the entries 0 or  $1/2$ . For instance, the two-scale relation of  $\phi_0$  at the level  $j = 0$  is given by

$$\begin{aligned} \phi_0(x) &= \phi_0(2x) + \phi_2(2x - \begin{pmatrix} 0 \\ 1 \end{pmatrix}) + \phi_3(2x - \begin{pmatrix} 0 \\ 1 \end{pmatrix}) + \phi_5(2x - \begin{pmatrix} 1 \\ 1 \end{pmatrix}) \\ &= \frac{1}{4\sqrt{2}} \left( \phi_{0,1,\begin{pmatrix} 0 \\ 0 \end{pmatrix}}(x) + \phi_{2,1,\begin{pmatrix} 0 \\ 1 \end{pmatrix}}(x) + \phi_{3,1,\begin{pmatrix} 0 \\ 1 \end{pmatrix}}(x) + \phi_{5,1,\begin{pmatrix} 1 \\ 1 \end{pmatrix}}(x) \right), \end{aligned}$$

see Figure 1(b). Now, we define multiwavelet vectors  $\Psi^l := (\psi_0^l, \dots, \psi_7^l)^T$  of multiplicity 8 by

$$\Psi^l(x) = 2 \sum_{k \in \mathbb{Z}^2} M_k^l \Phi(2x - k), \quad x \in \mathbb{R}^2, l = 1, 2, 3, \quad (2.1)$$

where the wavelet mask matrices  $M_k^l$  contain entries equal to  $0, 1/2$  and  $-1/2$ . Again we restrict ourselves to  $i = 0$ , where we get the wavelets

$$\begin{aligned} \psi_0^1 &:= \frac{1}{4\sqrt{2}} \left( \phi_{0,1,\begin{pmatrix} 0 \\ 0 \end{pmatrix}} + \phi_{2,1,\begin{pmatrix} 0 \\ 1 \end{pmatrix}} - \phi_{3,1,\begin{pmatrix} 0 \\ 1 \end{pmatrix}} - \phi_{5,1,\begin{pmatrix} 1 \\ 1 \end{pmatrix}} \right), \\ \psi_0^2 &:= \frac{1}{4\sqrt{2}} \left( \phi_{0,1,\begin{pmatrix} 0 \\ 0 \end{pmatrix}} - \phi_{2,1,\begin{pmatrix} 0 \\ 1 \end{pmatrix}} + \phi_{3,1,\begin{pmatrix} 0 \\ 1 \end{pmatrix}} - \phi_{5,1,\begin{pmatrix} 1 \\ 1 \end{pmatrix}} \right), \\ \psi_0^3 &:= \frac{1}{4\sqrt{2}} \left( \phi_{0,1,\begin{pmatrix} 0 \\ 0 \end{pmatrix}} - \phi_{2,1,\begin{pmatrix} 0 \\ 1 \end{pmatrix}} - \phi_{3,1,\begin{pmatrix} 0 \\ 1 \end{pmatrix}} + \phi_{5,1,\begin{pmatrix} 1 \\ 1 \end{pmatrix}} \right), \end{aligned}$$

according to Figure 2. Note, that it is possible to choose other coefficients in  $M_k^l$  instead of  $1/2$  and  $-1/2$ , but Roşca has shown in [11] that these wavelets are optimal with respect to image compression. More precisely, using a wavelet shrinkage to get an image approximation  $\tilde{f}$  for an image  $f$  our wavelets lead to a minimal approximation error  $\|f - \tilde{f}\|$ .

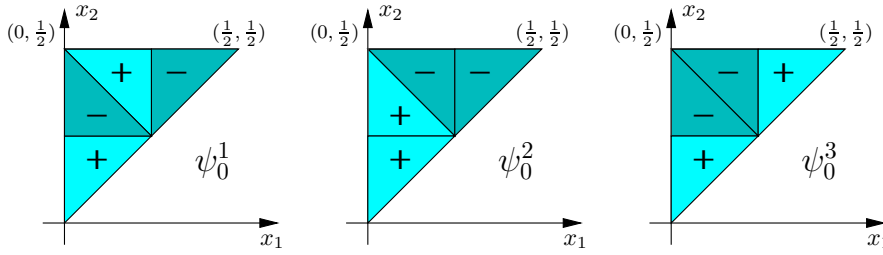


FIGURE 2. Wavelets.

Analogously to the scaling functions, the non-separable, directional wavelets can be represented as rotated resp. reflected versions of  $\psi_0^l$  for every  $i = 0, \dots, 7$ ,  $j \in \mathbb{Z}$  and  $k \in \mathbb{Z}^2$  through

$$\psi_{i,j,k}^l := 2^{j+1} \sqrt{2} \psi_0^l(B_i(2^j \cdot -k)), \quad l = 1, 2, 3.$$

Thus, we have for  $j \in \mathbb{Z}$  the wavelet spaces

$$W_j := \text{clos}_{L^2(\mathbb{R}^2)} \text{span}\{\psi_{i,j,k}^l : l = 1, 2, 3; i = 0, \dots, 7; k \in \mathbb{Z}^2\}.$$

Due to the refinement equation (2.1) we have  $W_j \subset V_{j+1}$ . Reconstruction formulas can now be derived as follows,

$$\begin{aligned} \phi_{0,j+1,2k} &= \frac{1}{2} (\phi_{0,j,k} + \psi_{0,j,k}^1 + \psi_{0,j,k}^2 + \psi_{0,j,k}^3), \\ \phi_{0,j+1,2k-\binom{1}{0}} &= \frac{1}{2} (\phi_{6,j,k} + \psi_{6,j,k}^1 - \psi_{6,j,k}^2 - \psi_{6,j,k}^3), \\ \phi_{0,j+1,2k-\binom{0}{1}} &= \frac{1}{2} (\phi_{3,j,k} - \psi_{3,j,k}^1 + \psi_{3,j,k}^2 - \psi_{3,j,k}^3), \\ \phi_{0,j+1,2k-\binom{1}{1}} &= \frac{1}{2} (\phi_{5,j,k} - \psi_{5,j,k}^1 - \psi_{5,j,k}^2 + \psi_{5,j,k}^3). \end{aligned}$$

The reconstruction formulas for the rotated and reflected functions follow analogously. Hence, we indeed have

$$V_j \oplus W_j = V_{j+1},$$

where the sum is orthogonal because the wavelet functions  $\psi_{i,j,k}^l$ ,  $l = 1, 2, 3$ , possess obviously the same compact support as the corresponding scaling functions  $\phi_{i,j,k}$  for all  $i, j, k$ . Thus, the entire system of directional wavelets

$$\{2^{j+1} \sqrt{2} \psi_i^l(2^j \cdot -k) : i = 0, \dots, 7, j \in \mathbb{Z}, k \in \mathbb{Z}^2, l = 1, 2, 3\} \quad (2.2)$$

generates an ONB for  $L^2(\mathbb{R}^2)$ , i.e.  $\bigoplus_{j \in \mathbb{Z}} W_j = L^2(\mathbb{R}^2)$ . Alternatively, one can also show the ONB property by arguments in the Fourier domain using the unitarity of the corresponding modulation matrix [1, Theorem 4.11] as well as the unitarity of the polyphase matrix [9].

### 3. Applications to image processing

In this section, we use our directional Haar wavelets on triangulations for denoising and approximation of images. Both methods are based on an efficient multiscale decomposition of images and a suitable wavelet shrinkage. Using our directional wavelet basis (2.2) we can represent an arbitrary function  $f \in L^2(\mathbb{R}^2)$  by  $f = \sum_{i,j,k} c_{i,j,k}^l \psi_{i,j,k}^l$ , where  $c_{i,j,k}^l = \langle f, \psi_{i,j,k}^l \rangle$  for  $i = 0, \dots, 7, j \in \mathbb{Z}, k \in \mathbb{Z}^2$ , and  $l = 1, 2, 3$ . Most of the information of the function  $f$  is carried by a small number of significantly large coefficients. These coefficients are typically concentrated near discontinuities of  $f$ . Therefore we get a good non-linear approximation  $f_\lambda$  of  $f$  by reconstructing from coefficients  $c_{i,j,k}^l$  above some threshold  $\lambda$

$$f_\lambda = \sum_{|c_{i,j,k}^l| \geq \lambda} c_{i,j,k}^l \psi_{i,j,k}^l.$$

The approximation error  $\|f - f_\lambda\|$  measures the quality of the approximation.

Let now  $a := (a_{i,j})_{i,j=0}^{N-1}$  be a discrete image with  $N \times N$  pixels. Its corresponding 'L<sup>2</sup>-version' can be understood as

$$f(x_1, x_2) = \sum_{k_1=0}^{N-1} \sum_{k_2=0}^{N-1} a_{k_1,k_2} \cdot \chi_{[0,1)^2}(x_1 - k_1, x_2 - k_2) = \sum_{k \in J} a_k \cdot \chi_{[0,1)^2}(x - k),$$

where  $\chi_{[0,1)^2}$  denotes the characteristic function on  $[0, 1)^2$  and  $J := \{0, \dots, N-1\}^2$ . Here, we assume that  $N = 2^{j_0}$  with a fixed  $j_0 \in \mathbb{N}$ .

In order to compute the multilevel representation of the image  $f$  from the fine to coarse scales, we propose as starting point for the decomposition algorithm an orthogonal projection  $f_{-1}$  of the image  $f$  into the space  $V_{-1}$ ,

$$f_{-1}(x) = \sum_{k \in J_1} c_k^T \sqrt{2} \Phi\left(\frac{1}{2}x - k\right), \tag{3.1}$$

preferring the vector notation with  $c_k := \langle f, \sqrt{2} \Phi(\frac{1}{2} \cdot -k) \rangle \in \mathbb{R}^8$  and  $J_1 := \{0, \dots, \frac{N}{2} - 1\}^2$ . In particular, the coefficient vectors are given by

$$c_k := \langle f, \sqrt{2} \Phi\left(\frac{1}{2} \cdot -k\right) \rangle = \sum_{l \in J} \sqrt{2} a_l \langle \chi_{[0,1)^2}(x - l), \Phi\left(\frac{1}{2} \cdot -k\right) \rangle,$$

where we can simply compute

$$\begin{aligned} \langle \chi_{[0,1)^2}(x - l), \Phi\left(\frac{1}{2} \cdot -k\right) \rangle &= \int_{[0,1)^2} \Phi\left(\frac{y+l}{2} - k\right) dy \\ &= \begin{cases} \frac{1}{2}(1, 1, 0, 0, 0, 0, 0, 0), & l = 2k \\ \frac{1}{2}(0, 0, 1, 1, 0, 0, 0, 0), & l = 2k + \begin{pmatrix} 0 \\ 1 \end{pmatrix} \\ \frac{1}{2}(0, 0, 0, 0, 1, 1, 0, 0), & l = 2k + \begin{pmatrix} 1 \\ 1 \end{pmatrix} \\ \frac{1}{2}(0, 0, 0, 0, 0, 0, 1, 1), & l = 2k + \begin{pmatrix} 1 \\ 0 \end{pmatrix} \\ 0, & \text{elsewhere} \end{cases} . \end{aligned}$$

Thus, the coefficient vector  $c_k$  in (3.1) is given by the pixels  $a_k$  of the image,

$$c_k^T = \frac{1}{\sqrt{2}} (a_{2k}, a_{2k}, a_{2k+\binom{0}{1}}, a_{2k+\binom{0}{1}}, a_{2k+\binom{1}{1}}, a_{2k+\binom{1}{1}}, a_{2k+\binom{1}{0}}, a_{2k+\binom{1}{0}}). \quad (3.2)$$

Having the projection  $f_{-1} \in V_{-1}$  we continue in a natural manner applying the filter bank algorithm, see [8] for details. According to our above remarks we completely decompose  $f_{-1}$  into wavelet coefficients and reconstruct it after a suitable shrinkage.

### 3.1. Image denoising

The coefficient vector in (3.2) contains eight entries which come from four pixel values. This double information is advantageous in image denoising. We consider a Gaussian noise with standard deviation  $\sigma = 15$  that is added to the  $256 \times 256$  synthetic image shown in Figure 3(a). We apply the directional Haar wavelet filter bank for decomposing the image. For the global hard-thresholding we choose the shrinkage parameter  $\lambda = \sigma \sqrt{\log(N^2)/2}$ , where  $N^2$  denotes the number of pixels. The complete decomposition of the image is given for  $j = 7$ . In comparison with the classical Haar filter (3(c)) we obtain good denoising results (see 3(d)) because the directional edges of the geometrical figures are well detected.

### 3.2. Image approximation

We decompose the image completely in its wavelet coefficients. Again, we use wavelet shrinkage with global hard-thresholding to get a sparse image representation. Here we choose the threshold  $\lambda$  such that only the five percent largest wavelet coefficients remain. In Figure 4 the approximations with 3277 coefficients of the  $256 \times 256$  'Elaine' detail image are displayed, comparing the classical Haar and Daubechies wavelet filter bank with our directional Haar filter bank. There are two reasons for the comparative low PSNR value. Firstly, there exists double redundancy (what is not desirable regarding sparse representation), and secondly, our Haar-type wavelets are not continuous.

## References

- [1] C. Cabrelli, C. Heil, and U. Molter, *Self-similarity and multiwavelets in higher dimensions*. *Memoirs Amer. Math. Soc.* **170**(807), 2004.
- [2] E.J. Candès and D.L. Donoho, *New tight frames of curvelets and optimal representations of objects with piecewise  $C^2$  singularities*. *Comm. Pure Appl. Math.* **56** (2004), 216–266.
- [3] M.N. Do and M. Vetterli, *The contourlet transform: an efficient directional multiresolution image representation*. *IEEE Trans. Image Process.* **14** (12) (2005), 2091–2106.
- [4] K. Gröchenig and W.R. Madych, *Multiresolution analysis, Haar bases, and self-similar tilings of  $\mathbb{R}^n$* . *IEEE Trans. Inform. Theory* **38** (1992), 556–568.
- [5] K. Guo and D. Labate, *Optimally sparse multidimensional representation using shearlets*. *SIAM J. Math. Anal.* **39** (2007), 298–318.

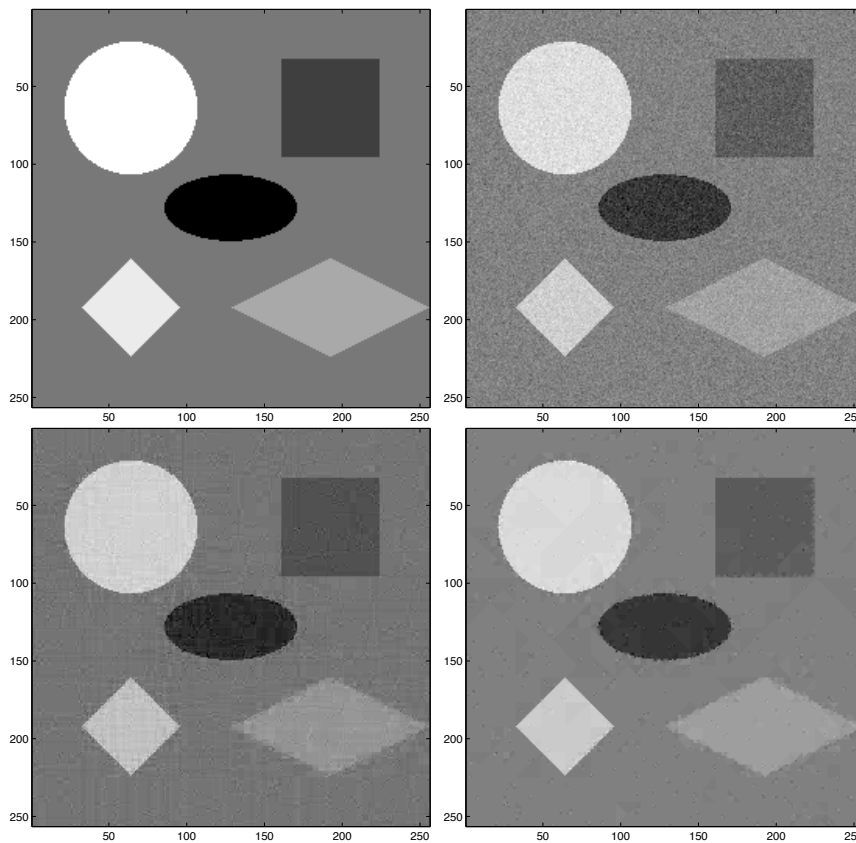


FIGURE 3. Denoising. (a) Original image, (b) noisy image, PSNR 24.58, (c) classical Haar, PSNR 30.31, (d) directional Haar, PSNR 33.81.

- [6] K. Guo, W.-Q. Lim, D. Labate, G. Weiss, and E. Wilson, *Wavelets with composite dilations and their MRA properties*. Appl. Comput. Harmon. Anal. **20** (2006), 231–249.
- [7] I. Krishtal, B. Robinson, G. Weiss, and E. Wilson, *Some simple Haar-type wavelets in higher dimensions*. J. Geom. Anal. **17** (2007), 87–96.
- [8] J. Krommweh and G. Plonka, *Directional wavelet frames on triangles*. Preprint, 2007. [http://www.uni-due.de/mathematik/krommweh/directional\\_frame.pdf](http://www.uni-due.de/mathematik/krommweh/directional_frame.pdf).
- [9] J. Krommweh, *Tight frame characterization of multiwavelet vector functions in terms of the polyphase matrix*. Int. J. Wavelets Multiresolut. Inf. Process. **7** (1) (2009), 9–21.
- [10] W.-Q. Lim, *Wavelets with Composite Dilations*. PhD thesis, Washington University, St. Louis, MO, 2005.



FIGURE 4. Approximation with 3277 coefficients. (a) Original 'Elaine' detail image, (b) classical Haar, PSNR 29.68, (c) Daubechies D4, PSNR 30.81, (d) directional Haar, PSNR 29.20.

- [11] D. Rosça, *Optimal Haar wavelets on spherical triangulations*. Pure Math. Appl. **15** (4) (2004), 429–438.

### Acknowledgment

The research in this paper is funded by the project PL 170/11-1 of the Deutsche Forschungsgemeinschaft (DFG). This is gratefully acknowledged. Furthermore the author would like to thank his advisor Gerlind Plonka for her helpful instructions and permanent support.

Jens Krommweh  
Department of Mathematics  
University of Duisburg-Essen, Campus Duisburg  
D-47048 Duisburg, Germany  
<http://www.uni-due.de/mathematik/krommweh/>  
e-mail: [jens.krommweh@uni-due.de](mailto:jens.krommweh@uni-due.de)